J. Fluid Mech. (1991), *vol.* 226, *pp.* 189–203
Printed in Great Britain

Inviscid free-surface flow over a periodic wall

By V. BONTOZOGLOU, S. KALLIADASIS AND A. J. KARABELAS

Chemical Process Engineering Research Institute and Department of Chemical Engineering, Aristotle University of Thessaloniki, PO Box 1517, GR 54006 Thessaloniki, Greece

(Received 23 January 1990 and in revised form 9 July 1990)

A numerical method is described, based on the hodograph formulation, for analysing inviscid, free-surface flows over a periodic wall. An efficient implementation of the wall boundary condition results in a straightforward method, accurate for a wide range of bottom undulation heights and flow parameters. It is demonstrated that a series of resonances is possible between the bottom undulations and the free surface. The steady, free-surface profiles are accurately calculated for a wide range of current velocities and are shown to be significantly dimpled by higher harmonics. A study of the flow field indicates that the free-surface shape strongly affects the velocities close to the wall, leading to distributions which change dramatically with current velocity. Some implications of the new results on the phenomena of wall dissolution or material deposition, Bragg scattering of surface waves and sediment transport in rivers, are discussed.

1. Introduction

An important class of problems in fluid mechanics involves flow over a wavy wall of a liquid bounded by a free-surface or fluid interface. Such flows, occurring both in nature and in chemical processes, are usually coupled with various transport phenomena, whose rate is strongly affected by the details of the flow field. Typical examples are river flow over an erodible bed, leading to sediment transport and deposition, and various processes involving heat and mass transfer in chemical engineering.

The existence of a free surface whose location is not known *a priori* poses severe mathematical difficulties, making the problem highly nonlinear. One simplification, customary in the study of natural flows and of plausible validity for thick films, is the neglect of viscosity. This approach, adopted in the present work, is known to provide an accurate description of free-surface flows. To this end it suffices to mention the recent comparison of Dommermuth *et al.* (1988), which demonstrated the agreement between experimental observations of plunging breakers and numerical computations based on potential theory (e.g. Longuet-Higgins & Cokelet 1976).

The specific problem considered in this article is the steady, inviscid flow of a liquid stream with uniform current velocity, over a periodic solid wall of given shape. Previous studies on the topic involved linear (Kennedy 1963; Reynolds 1965) and weakly nonlinear analysis of the steady flow (Miles 1986). In the present study a numerical computation is performed, valid for wall undulations of finite amplitude and free-surface waves of any steepness. Specifically addressed are the effects of current velocity and disturbance height on the free-surface morphology and the flow

structure, with emphasis on the velocity distribution along the wall. The results include exact calculation of the free-surface profiles, which occasionally exhibit a complexity not intuitively evident. The flow field close to the wall is shown to change drastically with current velocity, a result with important implications for sediment transport and wall dissolution phenomena.

The related inverse problem, which involves constructing free-surface solutions with corrugated streamlines, has been studied by – among others – Richardson (1920) and John (1953) (for a review see Wehausen & Laitone 1960). These results are evidently less useful, since they involve very specific boundary shapes which, in addition, are dictated by the solution itself. A family of steady flows discovered by John (1953) has been calculated in the present work as a direct problem in order to test the accuracy of the numerical scheme.

The flow of interest is analysed in the hodograph formulation (devised by Stokes 1880) whereby the location of a point in the fluid domain is cast as a Fourier series in the velocity potential ϕ and the stream function ψ. This approach allows direct application of the kinematic boundary conditions and exhibits better convergence characteristics for steep profiles than the physical formulation (Saffman & Yuen 1982). Although the present work involves only gravity waves, the numerical method is generalized with the inclusion of surface tension. The implementation of the bottom boundary condition is a non-trivial task and an interesting Fourier-inversion formulation is adopted to assure proper convergence.

The problem is formulated in §2 and the numerical method developed and evaluated in §3. The free-surface morphology is examined in §4 and the flow field in §5. Finally, §6 contains some concluding remarks.

2. Formulation of the problem

Periodic, stationary waves are considered on the free surface of a liquid, which is flowing over a periodic boundary. The liquid is taken to be incompressible and inviscid and the motion irrotational. Solutions are obtained for two-dimensional waves, with wavelength equal to that of the bottom wall disturbance and in phase (or 180° out of phase) with it. Units of length, mass and time are chosen so that the wavelength $L = 2\pi$, the fluid density $\rho = 1$ and the gravitational acceleration $g = 1$. Equivalently, all lengths are non-dimensionalized with the wavenumber k and the velocities are Froude numbers using k^{-1} as characteristic length.

The flow is sketched in figure 1. Rectangular coordinates (x, y) are chosen such that the x-axis is horizontal and the y-axis directed vertically upward. The interface is located at $y = \eta$ and the origin is such that the mean elevation $\bar{\eta}$ is zero. The bottom boundary consists of sinusoidal disturbances of amplitude α. Its average elevation, $-D$, in the above coordinate system, is taken as the mean depth of the liquid. The stream is moving with ambient velocity U, defined as the horizontal velocity averaged over one cycle on any fixed height within the liquid. With the above formulation the equations that need to be satisfied are Laplace's equation in the domain, the kinematic and dynamic boundary conditions on the free surface and the no-penetration condition on the bottom wall.

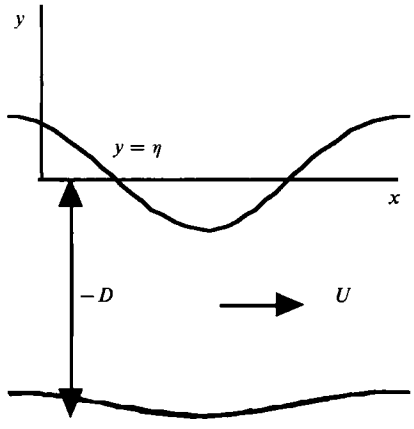

FIGURE 1. Sketch of the flow considered.

3. Numerical method

3.1. *Hodograph formulation*

A velocity potential ϕ and a stream function ψ are considered for the liquid and the following complex variables are defined:

$$z = x + \mathrm{i}y, \quad w = \phi + \mathrm{i}\psi. \tag{3.1}$$

With the above definitions, z can be expanded as a Fourier series in w, truncated to order N:

$$z = A_0 \frac{w}{U} + B_0 + \sum_{j=1}^{N} (A_j \mathrm{e}^{\mathrm{i}jw/U} + B_j \mathrm{e}^{\mathrm{i}jw/U}), \tag{3.2}$$

where the velocity field is given by

$$u - \mathrm{i}v = \frac{\mathrm{d}w}{\mathrm{d}z} = \left(\frac{\mathrm{d}z}{\mathrm{d}w}\right)^{-1} \tag{3.3}$$

and A_j, B_j, A_0, B_0 are in general complex. Considering only waves symmetric about the crest, applying the definition of the ambient velocity U and splitting into real and imaginary parts, the following are derived:

$$x = \xi + \sum_{j=1}^{N} (a_j \mathrm{e}^{j\psi/U} - b_j \mathrm{e}^{-j\psi/U}) \sin(j\xi), \tag{3.4a}$$

$$y = \frac{\psi}{U} - H + \sum_{j=1}^{N} (a_j \mathrm{e}^{j\psi/U} + b_j \mathrm{e}^{-j\psi/U}) \cos(j\xi), \tag{3.4b}$$

where a_j, b_j and H are real and $\xi = \phi/U$. The stream function is taken as $\psi = 0$ along the free surface and $\psi = Q$ on the wall, where $|Q|$ is the volume flow rate per unit span.

$$\left.\begin{aligned} \psi &= 0 \quad \text{on} \quad y = \eta, \\ \psi &= Q \quad \text{on} \quad y = D + \alpha \cos x. \end{aligned}\right\} \tag{3.5}$$

The term H is calculated by requiring that the average free-surface elevation be zero. The average elevation is found by substituting $\psi = 0$ in (3.4b) and integrating over one wavelength:

$$\bar{\eta} = \frac{1}{\pi} \int_0^{\pi} y \left(\frac{\mathrm{d}x}{\mathrm{d}\xi}\right)_{\psi=0} \mathrm{d}\xi = -H + \frac{1}{2} \sum_{j=1}^{N} j(a_j^2 - b_j^2). \tag{3.6a}$$

Setting $\bar{\eta} = 0$ gives

$$H = \frac{1}{2}\sum_{j=1}^{N} j(a_j^2 - b_j^2). \tag{3.6b}$$

The term $d = Q/U$ is an equivalent depth and in general differs from the mean depth D. These quantities are related by calculating the average bottom elevation (same procedure as (3.6a, b)), subtracting it from the average free-surface elevation and setting the difference equal to $|D|$:

$$-d + \frac{1}{2}\sum_{j=1}^{N} j[a_j^2(1-e^{2jd}) - b_j^2(1-e^{-2jd})] = |D|. \tag{3.7}$$

3.2. *Numerical solution–performance*

The equations to be satisfied in the above formulation are the dynamic boundary condition along the free surface and the geometric requirement that the streamline $\psi = Q$ coincide with the bottom wall. Applying Bernoulli's equation, the dynamic boundary condition is brought to the form

$$-\tfrac{1}{2}q^2 + \eta - \kappa R^{-1} = B, \tag{3.8}$$

where κ is a dimensionless surface tension, equal to $4\pi^2\sigma/\rho g L^2$, σ is the dimensional surface tension and B is Bernoulli's constant.

The term R is the radius of curvature of the interface and its inverse equals

$$R^{-1} = \frac{d^2\eta/dx^2}{[1+(d\eta/dx)^2]^{\frac{3}{2}}} = \frac{x'y'' - x''y'}{(x'^2+y'^2)^{\frac{3}{2}}}, \tag{3.9}$$

where x', y' etc. are derivatives with respect to ξ of the interface coordinates x, y. Equation (3.8) is discretized by $N+1$ points from crest to trough using $\xi_i = (i-1)\pi/N$, $i = 1, \ldots, N+1$.

The geometric requirement for the bottom wall can be formulated as

$$(y)_{\psi=Q} - D = \alpha \cos(x)_{\psi=Q}, \tag{3.10}$$

where x, y are derived from (3.4a, b) by substituting $\psi = Q$. Equation (3.10) could in principle be discretized to provide the rest of the equations needed to define the unknowns $a_j, b_j, j = 1, \ldots, N$. Such a formulation, however, was pursued and gave meaningless solutions. Indeed, an anomalous increase was observed in the amplitudes of the last few harmonics which persisted with increasing values of N. Furthermore, the results depended on N. It was speculated that the discretization along both the bounding wall and the free surface permitted the intrusion of physically meaningless high-frequency harmonics, which would be excluded if (3.10) was somehow satisfied at every point along the boundary. It will be noted that application of the hodograph formulation with a flat wall, where (3.10) can be implemented analytically, never met with similar difficulties.

To circumvent the problem the following procedure is pursued. Equation (3.10) is considered as a Fourier series in $\cos j\xi$ of the form

$$\sum_{j=1}^{N} (a_j e^{jd} + b_j e^{-jd}) \cos j\xi = \alpha \cos(x)_{\psi=Q}. \tag{3.11}$$

The Euler–Fourier formula for finding the coefficients of the series is applied, giving

$$a_j e^{jd} + b_j e^{-jd} = \frac{2}{\pi}\int_0^{\pi} [\alpha \cos(x)_{\psi=Q}] \cos j\xi \, d\xi, \quad j = 1, \ldots, N. \tag{3.12}$$

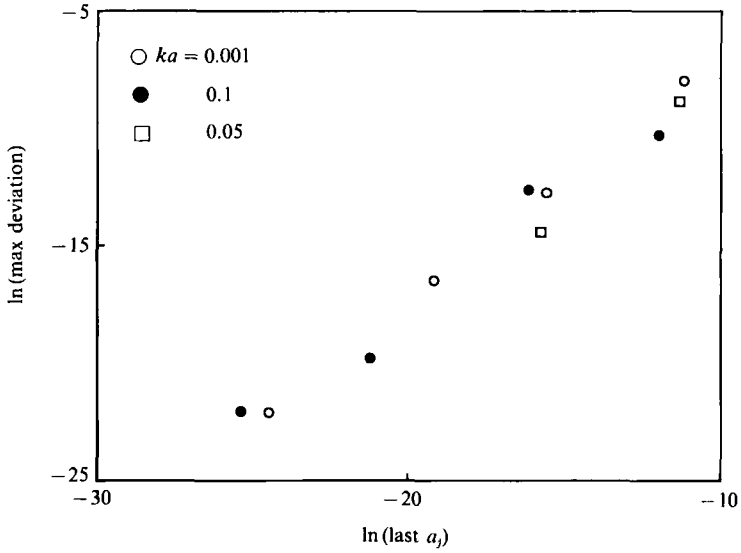

FIGURE 2. The maximum of the residuals at non-nodal points versus the magnitude of the last Fourier coefficient. A strong correlation is shown to hold for the entire range of bottom undulations.

The above N equations are used to close the system. Together with the $N+1$ equations resulting from the discretization of (3.8), they provide a system of $2N+1$ equations in the $2N+1$ unknowns $a_1, \ldots, a_N, b_1, \ldots, b_N, B$. If the mean, instead of the equivalent depth is considered as the input parameter (as is done in the present work), d is introduced as an additional unknown and (3.7) is the last equation needed.

The system of equations is solved by Newton's method. Typically, three to four iterations are needed to achieve convergence. Accuracy is tested by the independence of the results of the value of N and the error is monitored by the magnitude of the last Fourier coefficient. As an additional test, the residuals at non-nodal points were checked for representative runs. The results, plotted in figure 2, indicate that the maximum deviations scale very well with the magnitude of the last Fourier coefficient.

The method works extremely well for a wide range of parameter values. Away from resonances a few harmonics are sufficient to describe the flow. Higher resolution, however, is needed near resonance and with increased bottom steepness. The bulk of the results presented in this work were derived using 16 or 24 harmonics.

3.3. *Comparison with exact solutions*

John (1953), considering two-dimensional flows described by a complex velocity potential $F(z)$ ($z = x + \mathrm{i}y$), discovered the following solution family which corresponds to flow with corrugated streamlines:

$$\left.\begin{aligned} z &= \frac{g}{v}\tau + A\,\mathrm{e}^{\mathrm{i}v\tau} \\ F(z) &= \left(\frac{g^2}{v^2} + A^2v^2\right)\tau + \frac{2gA}{v}\cos v\tau. \end{aligned}\right\} \tag{3.13}$$

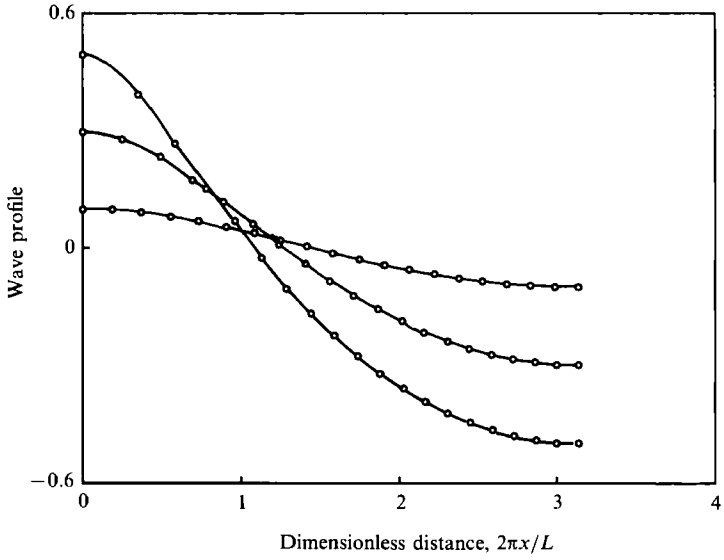

FIGURE 3. Comparison between numerical computations (circles) and analytic solution (lines) based on John's (1953) inverse method.

Term g is the gravitational constant, v is real-positive and the free surface is recovered for real values of τ. For $A < g/v^2$ the surface is a simple periodic curve of amplitude A and wavelength $L = 2pg/v^2$. Branch points occur at the positions

$$z_n = (n+\tfrac{1}{4})L + \frac{\mathrm{i}}{2\pi}\left(1 - \log\frac{L}{2\pi A}\right)L, \quad n \in N \tag{3.14}$$

and any streamline above or through the branch points can be taken as the bottom surface.

The above steady flows are recalculated in the present work as a direct problem in order to test the accuracy of the proposed numerical scheme. The ambient current velocity used in the numerical computations is found (by integration of the velocity vector along the free surface and use of Stokes theorem) to equal

$$U = \frac{g}{v} + \frac{A^2 v^3}{g}. \tag{3.15}$$

The mean depth D corresponding to the analytic solutions is also calculated and representative runs are performed. Figure 3 shows the free-surface profiles calculated analytically and numerically for $2\pi A/L = 0.1$, 0.3 and 0.5, using as the bottom the streamlines through the branch points. The agreement observed demonstrates the accuracy of the numerical scheme used.

4. Free-surface profiles

The waviness of the solid wall causes deflection of the streamlines, which affects the shape of the free surface. In the present section, flow without capillary forces is analysed, concentrating on the effect of disturbance amplitude and current velocity. Examining the morphology of the free surface is certainly of interest from a fundamental standpoint. Additionally, it serves as an input for a more detailed

consideration of the structure of the flow, a task which is undertaken in the next section. The results which follow might also have some bearing on the approach to Bragg scattering of surface waves over a periodic bottom topography (Davies & Heathershaw 1984; Hara & Mei 1987), as is discussed in more detail in §6.

Before presenting the numerical results it is instructive to recall some conclusions of linear theory. The linearized problem for small wall amplitude has been considered by Reynolds (1965). In the notation of figure 1, the following free-surface profile is obtained:

$$n(x) = a\cos kx \frac{U^2}{\cosh kD(k/gU^2 - \tanh kD)}. \tag{4.1}$$

The free-surface, therefore, is sinusoidal with height that is not necessarily smaller than the wall disturbance (contrast with creeping flow; e.g. Pozrikidis 1988). The perturbed flow field has a singularity at the zero of the denominator of (4.1), which corresponds to a current velocity

$$U_{\text{res}}^2 = g/k \tanh kD \tag{4.2}$$

reminiscent of the dispersion relation for water waves. This indicates a resonance between a free-surface wave (stationary, riding on a current) and the bottom forcing. Crossing the singular current velocity is accompanied by a jump in the phase of the free-surface wave. Small currents create surface waves 180° out of phase with the bottom disturbance, whereas large currents lead to surface waves in phase with the bottom wall.

Miles (1986) showed that the singularity may be removed by including second-order effects. His analysis is limited to the neighbourhood of the resonance, positing a scaling of the wall amplitude α, relative to the wave amplitude a of the order $\alpha = O(a^3)$. Furthermore, the scaling $\alpha_N = O(a^N)$ is assumed for the wave harmonics. According to this weakly nonlinear analysis, the resonance curve of wave amplitude versus current velocity is triple-valued in some range of current velocities. The curve comprises two turning points, with the intermediate branch being always unstable. It should also be noted that excluding phenomenological damping, as is the case with the present work, moves one of the turning points to infinity.

The numerical method developed is presently applied to study the free-surface configuration for a wide range of parameter values. The goal is to accurately describe steep waves as well as investigate the possibility of different free-surface configurations, by relaxing the scaling assumed in Miles' weakly nonlinear analysis.

A dimensionless water depth $kD = 0.5$ is chosen as a case study. A bottom disturbance with steepness $k\alpha = 0.001$ is studied first. The numerical results for this small amplitude provide a proper framework for comparisons with weakly nonlinear theory. The magnitude of the free-surface wave is examined in a quantitative fashion by constructing the resonance curve of wave amplitude versus current velocity. Velocity U is used as the continuation parameter up to the turning point of the resonance curve. Beyond this point the formulation is recast, with U as an unknown and the wave steepness, ka, as the input parameter. The results are illustrated in figure 4, where close agreement between the numerical and analytical solution is observed for waves of small to intermediate height. It is interesting to note that discrepancies occur for $ka = O(0.1)$, which corresponds to the limit of validity of the scaling $\alpha = O(a^3)$ assumed by Miles. The numerical results demonstrate a steeper ascent of the resonance curve than predicted by second-order analysis. This observation is actually valid for higher wall corrugations as well (see figure 5).

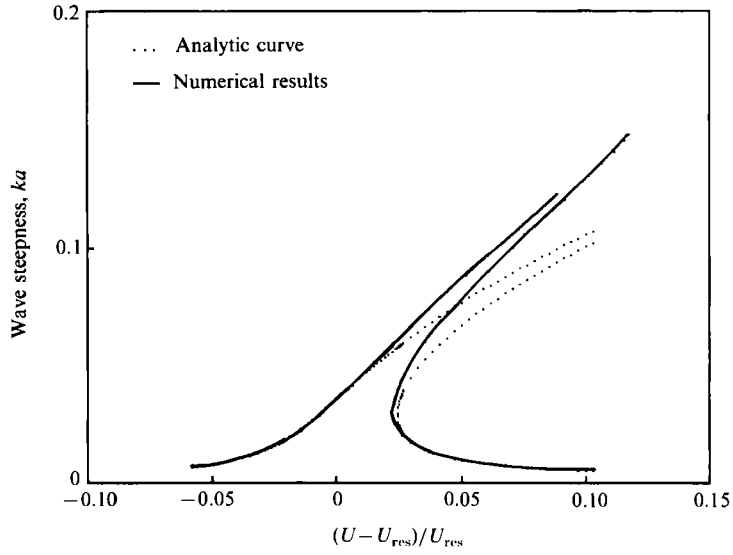

FIGURE 4. Part of the resonance curve of wave amplitude versus current velocity for undulations with steepness $k\alpha = 0.001$. Close agreement is observed in the neighbourhood of the resonant velocity.

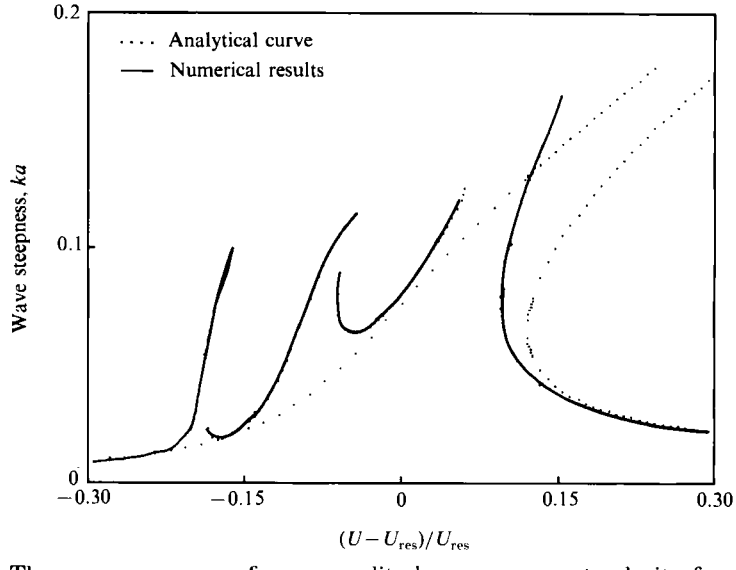

FIGURE 5. The resonance curve of wave amplitude versus current velocity for undulations with steepness $k\alpha = 0.01$.

Results for bottom disturbance with steepness $k\alpha = 0.01$ are presented next. The disturbance is still 'small' but serves to indicate an unexpected versatility of profiles emanating from higher-order resonances. The resonance curve of wave amplitude versus current velocity is again constructed and illustrated in figure 5. The numerical results are seen again to deviate from the analytic approximation around the main resonance. Even more important, triple-valued solution branches are also evident in the neighbourhood of $U \approx 0.91U_{res}$ and $U \approx 0.81U_{res}$. These current velocities

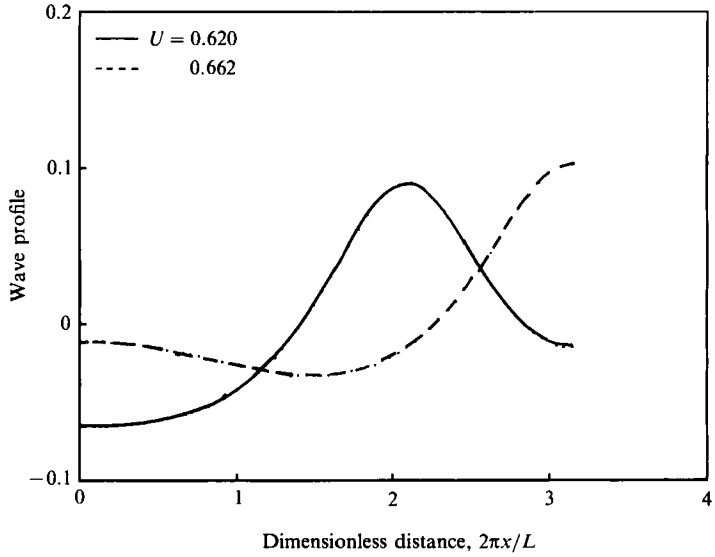

FIGURE 6. Typical surface profiles for current velocities in the neighbourhood of the second resonance. Note that, since the profiles are always symmetric about the crest or trough, only one half is presented ($x = 0$ to $x = \frac{1}{2}L$) here and in the following figures. The dimensionless velocity U is a Froude number, using $1/k$ as characteristic length. Also note that the resonant velocity from linear theory corresponds to $U = 0.680$.

correspond to the phase speed of free-surface waves with wavelengths half and one third of the wall disturbance, respectively. The singularities are thus due to resonances of the free wave with higher harmonics of the boundary forcing. Evidently there exists a whole class of such resonances, consisting of the superharmonics of the fundamental disturbance. It is noted though that, as the harmonic of interest increases in order, the dimensionless depth kD increases as well, approaching asymptotically the deep-water limit. The resonances therefore are expected to become increasingly weaker. This is evident in figure 5, where the range of current velocities over which very steep free-surface waves exist is observed to shrink with increasing order of the resonance.

A profound change in the morphology of the free surface takes place for current velocities around the resonant values. This is illustrated in figure 6, where free-surface profiles are plotted for current velocities around $0.91U_{\text{res}}$. It is evident that a strong second harmonic has developed, resulting in a dimpled profile. The dimple is located at the crest in the solution branch coming from small current velocities and at the trough in the order one.

Increasingly complex profiles appear in the neighbourhoods of the higher resonances, typical examples of which are plotted in figure 7. The superharmonics deform the sinusoidal wave profile for a considerable range of current velocities, and dominate the main harmonic close enough to the resonance. It should be noted, however, that for no current velocity in the present work did the amplitude of the first harmonic reduce to zero, so that a gradual transition from a wave with wavelength L to one with $\frac{1}{2}L$ did not take place. The possibility, therefore, of a subharmonic bifurcation, similar to the one reported for capillary–gravity water waves (Chen & Saffman 1979) is not supported.

As a final example of the capabilities of the computational scheme, some free-

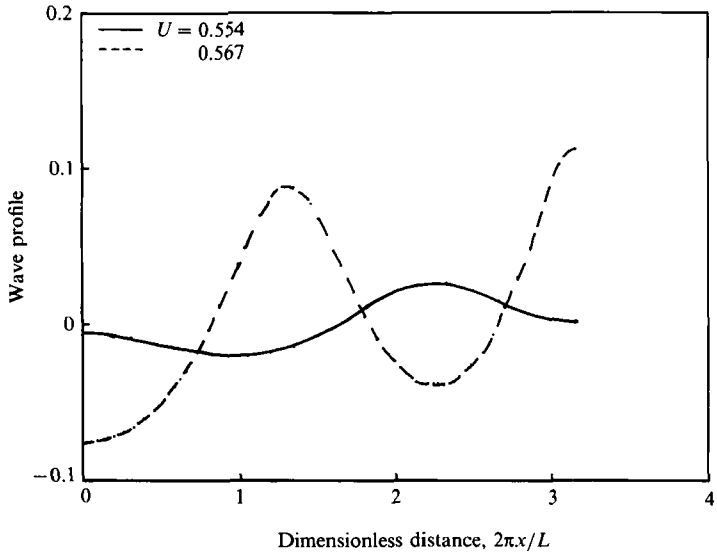

FIGURE 7. Typical surface profiles for current velocities around the third resonance. An increased degree of complexity is evident.

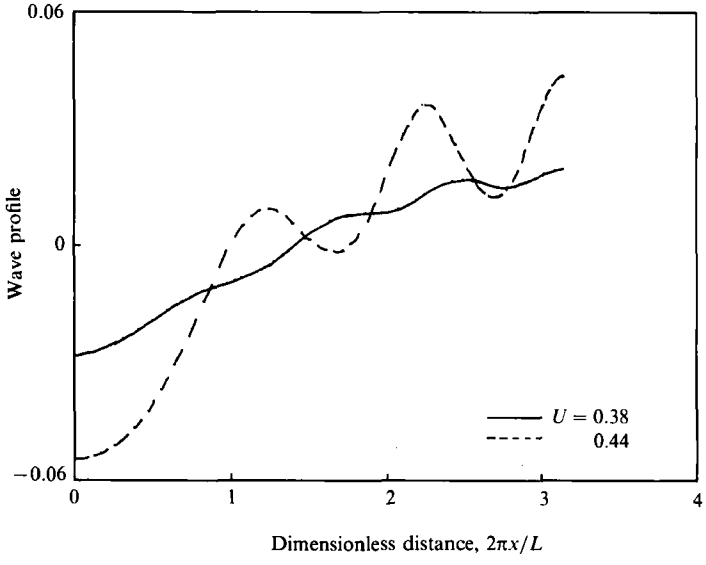

FIGURE 8. Free-surface profiles for bottom steepness $k\alpha = 0.05$. With increasing disturbance height, such highly dimpled profiles are observed for a wider range of current velocities.

surface profiles for bottom disturbance with steepness 0.05 are presented in figure 8. One consequence of the increased modulation height is the extension of the current velocity range over which superharmonics are evident on the wave profiles. Highly dimpled profiles, like the ones presented in figure 8, are now observed for a significant range of velocities.

The shape of the resonance curve, with continuously increasing wave amplitude poses the question of a geometric limit. Numerical evidence for the existence of such

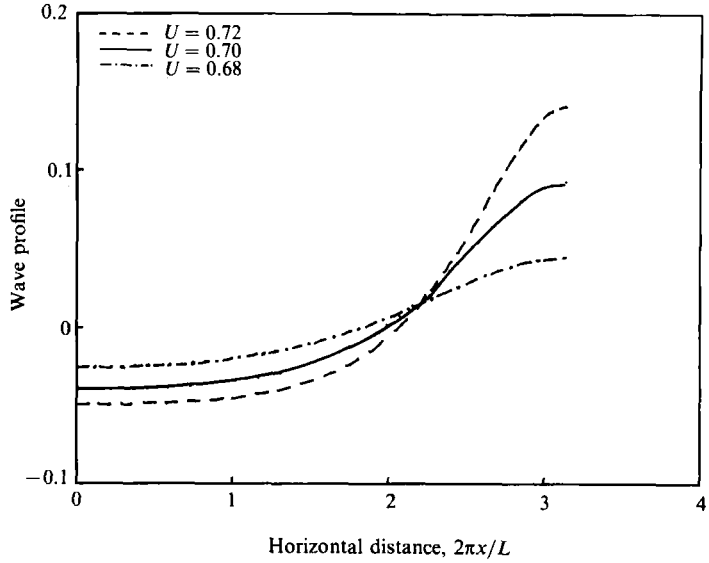

FIGURE 9. Large-amplitude profiles for wall steepness $k\alpha = 0.001$. The approach to a geometrical limit is evident.

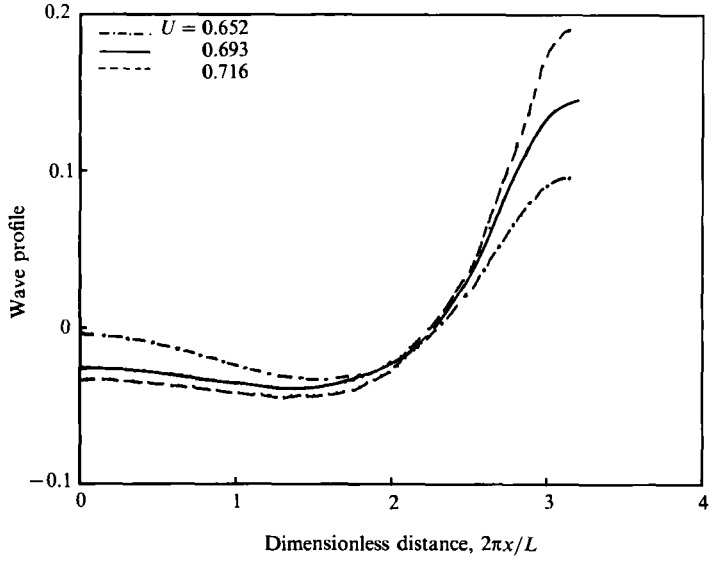

FIGURE 10. Profiles with increasing amplitude along the first resonance curve, for $k\alpha = 0.01$.

a limit is presented in figures 9 and 10. For wall disturbance with steepness $k\alpha = 0.001$, figure 9 indicates that a sharp corner develops at the crest, as one moves along the resonance curve. The shape is very close to Stokes free-surface wave, which is evidently the asymptotic limit for $k\alpha \to 0$, $U \to U_{res}$. Figure 10 shows steep waves along the first resonance branch, for $k\alpha = 0.01$. The profiles again tend to peak at the crest. Note however that a dimple at the trough persists even for current velocities considerably distant from the second-order resonance.

5. Structure of the flow

In the previous section, the amplitude and shape of the free surface was examined as a function of current velocity, for wall disturbances of various heights. The present section elucidates some aspects of the flow structure, focusing on the velocity distribution along the wall (slip velocity).

The slip velocity, calculated from the present inviscid approximation, provides essential information for understanding processes that take place close to the wall. Its distribution and rate of change dictate the velocity profile across the boundary layer as well as its thickness. It is, therefore, of central importance in problems involving heat or mass transfer. The problem of sediment transport and deposition along a river is also relevant to the present study, since the sediment carrying ability of the flow is generally related (mostly empirically) to the local velocity field close to the river bottom (Reynolds 1965; Engelund & Fredsøe 1982).

Before presenting numerical results for the intermediate range of current velocities, it is instructive to consider the asymptotic limit of very low flow rates. For current velocities approaching zero the free surface is slightly deflected from horizontal and the flow field along the bottom wall is determined predominantly by the wall shape itself. This is demonstrated in figure 11 for one mild and one steep wall disturbance. The slip velocity varies in phase with wave height, as is intuitively expected from a consideration of the Bernoulli effect. Weakly nonlinear theory predicts that, by increasing the current velocity, this variation of the bottom velocity persists and becomes more pronounced. This is so because the free-surface waves, whose height increases with the approach to the resonance velocity $U_{\rm res}$, are 180° out of phase with the wall disturbance and thus amplify the Bernoulli effect. Inclusion of higher-order effects, as in the numerical results to be presented next, considerably alters this picture.

Slip velocity distributions for some current velocities $U < U_{\rm res}$ and wall disturbance with steepness $k\alpha = 0.01$ are depicted in figure 12. One striking result is that the curve loses the sinusoidal form, with the velocity maximum shifting in some cases downstream from the crest, and the minimum upstream in others. Examination of the pertinent free-surface profiles (figures 6 and 7) reveals that the velocity extrema are associated with variations of the liquid film thickness imposed by the shape of the free-surface profile. It should indeed be noted that in all our calculations, both the free-surface and the bottom tangent velocities roughly scale with the liquid depth. Consequently, knowing the surface profile enables one to estimate the slip velocity by a simple mass balance.

Numerical results for the other asymptotic limit, namely very high flow rates, are in agreement with the second-order theory and are hence briefly summarized. For very high current velocities, associated with insignificant surface deflection, the slip velocity distribution is in phase with the bottom height. As the current velocity decreases approaching the resonant value, the height of the free-surface profile increases far beyond that of the bottom undulations, while it remains in phase with them. Consequently, the slip velocity distribution presents maxima on the wall troughs and minima on the crests. Evidently, there exists an intermediate range of current velocities over which the slip velocity is almost uniform along the periodic wall.

Finally, the question is examined of whether the bottom undulations have a net effect on the volumetric flow rate of the liquid stream. The volumetric flow rate can be easily derived from the numerical results, since the equivalent depth d is part of

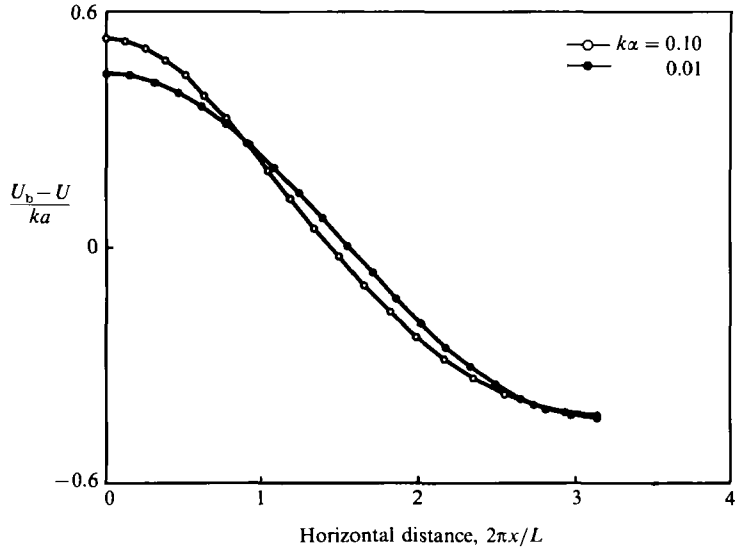

FIGURE 11. Velocity distribution along the bottom wall, for current velocity approaching zero. The variation of the slip velocity, U_b, from the ambient, U, scales with the wall steepness, as predicted by a local Bernoulli effect.

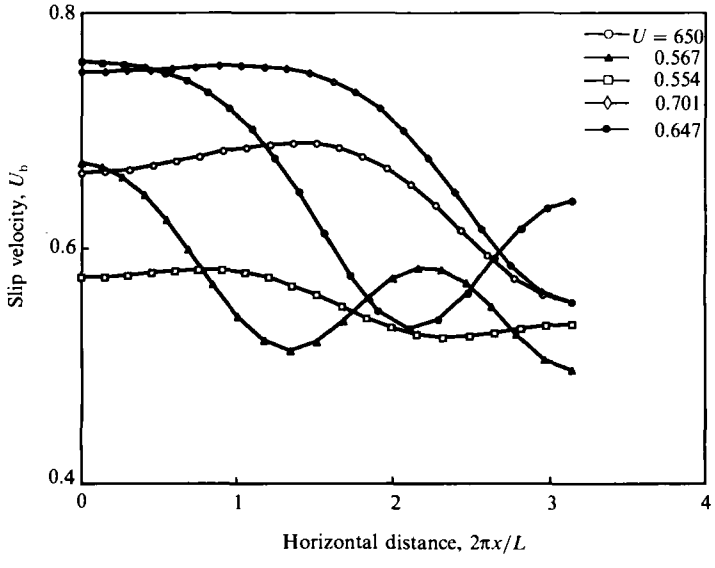

FIGURE 12. Wall velocity distributions for subresonant current velocities and $k\alpha = 0.01$.

the solution. The flow rate, then, is calculated as $Q = U|d|$ and compared with $Q_0 = U|D|$, which corresponds to undisturbed flow with the same average liquid depth. Some results are shown in figure 13 for $k\alpha = 0.01$ and 0.10. They indicate that the bottom waves always lead to a decrease in the flow rate which, however, becomes significant only for current velocities around the resonant ones. This change in the flow rate turns out to be an $O(\alpha^2)$ effect, so it might be important for wall undulations that are steep enough. This phenomenon could have interesting implications as in the case when flow over undulations is preceded by flow over a flat bottom. The present approach then needs to be coupled with a viscous force balance, providing a relation

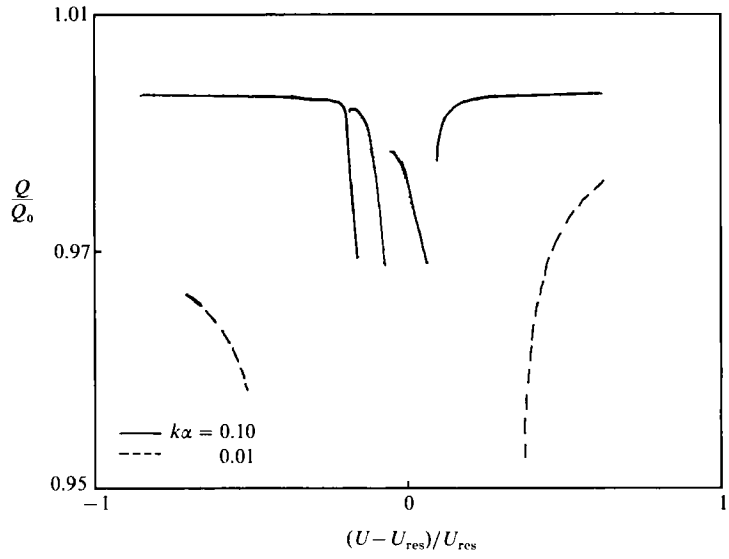

FIGURE 13. The volumetric flow rate as a function of current velocity, for undulations with steepness $k\alpha = 0.01$ and 0.10.

between the flow-driving force and the film height and average velocity, the last two being considered independent variables in the inviscid approach. Such an analysis, however, is beyond the scope of this work.

6. Concluding remarks

A numerical method has been described, based on the hodograph formulation, for analysing inviscid, free-surface flows over a periodic bottom. An efficient implementation of the wall boundary condition resulted in a straightforward method, accurate for a wide range of bottom undulation heights and flow parameters.

A number of interesting results emerged from the present work. It was demonstrated that a series of resonances is possible between the bottom undulations and the free surface. The steady, free-surface profiles were accurately calculated for a wide range of current velocities and were shown to be significantly dimpled by higher harmonics. This result could have some bearing on the approach to Bragg scattering of surface waves over periodic bottom topography. In particular, the effect of an ambient current velocity on the reflective characteristics of undular bottom has been studied in a linearized context (Kirby 1988), where it is assumed that the bottom disturbance contributes to the resonant triad a stationary wave of the same wavelength as the topography. The present study shows that a considerably more complex surface structure is possible for some ranges of current velocity, even for mild slopes of the bottom undulations. This result implies that waves with wavelength equal to a fraction of the fundamental will also be reflected to a considerable extent. The authors of the present work, however, are unaware of any experiments concerning current effects on Bragg resonance, which could test the above prediction.

A study of the flow field indicated that the free-surface shape strongly affects the velocities close to the wall, leading to distributions which change dramatically with current velocity. These results could have implications for the phenomenon of

sediment transport in rivers. Although a detailed examination of the phenomenon is beyond the scope of the present work, it is interesting to note that our new results concern the subcritical flow regime, which was proven the most difficult to model by linear potential theory (Engelund & Fredsøe 1982).

One particular observation, concerning the velocity distribution close to the bottom for subcritical currents, is the occasional shift of the slip velocity extrema from the crest and trough of the disturbance. It is expected that this shift will have a pronounced effect on the evolution of the wall shape in phenomena involving wall dissolution or material deposition. It is envisioned that modelling efforts could involve a quasi steady-state approximation, whereby the flow field calculated by the present methods (possibly supplemented by a boundary-layer analysis) for an initial bottom configuration would be substituted in a diffusion equation to derive the evolution of the configuration over a small time interval, and so on. Although quantitative assessment should await this or a similar analysis, it can be speculated that the wall evolution will be fairly complicated and will result in a moving, rather than a stationary, bottom configuration.

This work has been supported in part by the General Secretariat for Research and Technology of Greece and by the Commission of European Communities (under the programme VALOREN).

REFERENCES

CHEN, B. & SAFFMAN, P. G. 1979 Steady gravity–capillary waves on deep water. I. Weakly nonlinear waves. *Stud. Appl. Maths* **60**, 183.

DAVIES, A. G. & HEATHERSHAW, A. D. 1984 Surface-wave propagation over sinusoidally varying topography. *J. Fluid Mech.* **144**, 419.

DOMMERMUTH, D. G., YUE, D. K. P., LINN, W. M., RAPP, R. J., CHAN, E. S. & MELVILLE, W. K. 1988 Deep-water plunging breakers: a comparison between potential theory and experiments. *J. Fluid Mech.* **189**, 423.

ENGELUND, F. & FREDSØE, J. 1982 Sediment ripples and dunes. *Ann. Rev. Fluid Mech.* **14**, 13.

HARA, T. & MEI, C. C. 1987 Bragg scattering of surface waves by periodic bars: theory and experiment. *J. Fluid Mech.* **178**, 221.

JOHN, F. 1953 Two-dimensional potential flows with a free boundary. *Commun. Pure Appl. Maths* **6**, 497.

KENNEDY, J. F. 1963 The mechanisms of dunes and unitdunes in erodible-bed channels. *J. Fluid Mech.* **16**, 521.

KIRBY, J. T. 1988 Current effects on resonant reflection of surface water waves by sand bars. *J. Fluid Mech.* **186**, 501.

LONGUET-HIGGINS, M. S. & COKELET, E. D. 1976 The deformation of steep surface waves on water. I. A numerical method of computation. *Proc. R. Soc. Lond.* A **350**, 1.

MILES, J. W. 1986 Weakly nonlinear Kelvin–Helmholtz waves. *J. Fluid Mech.* **172**, 513.

POZRIKIDIS, C. 1988 The flow of a liquid film along a periodic wall. *J. Fluid Mech.* **188**, 275.

REYNOLDS, A. J. 1965 Waves on the erodible bed of an open channel. *J. Fluid Mech.* **22**, 113.

RICHARDSON, A. R. 1920 Stationary waves in water. *Phil. Mag.* **40**, 97.

SAFFMAN, P. G. & YUEN, H. C. 1982 Finite-amplitude interfacial waves in the presence of a current. *J. Fluid Mech.* **123**, 459.

STOKES, G. G. 1880 *Scientific Papers*, vol. 1, p. 227. Cambridge University Press.

WEHAUSEN, J. V. & LAITONE, E. V. 1960 Surface waves. *Handbuch der Physic*, vol. 9, p. 739. Springer.